

Influence of chemical schemes, numerical method and dynamic turbulent combustion modeling on LES of premixed turbulent flames.

B. Rochette^{1 2}, F. Collin-Bastiani^{1 3}, L. Gicquel¹, O. Vermorel¹, D. Veynante⁴, T. Poinsot⁵

Abstract

This paper describes Large Eddy Simulations of a turbulent premixed flame (the VOLVO rig) comparing Analytically Reduced Chemistry (ARC) [1] with globally reduced chemistry for propane-air combustion, a dynamic Thickened Flame (TFLES) model [2, 3] with the usual non-dynamic TFLES model [4] and a high-order Taylor Galerkin numerical scheme [5] with a low-order Lax-Wendroff scheme [6]. Comparisons with experimental data are presented for a stable case in terms of velocity and temperature fields. They show that going from two-step to ARC chemistry changes the flame stabilization zone. Compared to the usual non-dynamic TFLES model, the dynamic formulation allows to perform a parameter-free simulation. Finally, the order of accuracy of the numerical method is also found to play an important role. As a result, the high-order numerical method combined with the ARC chemistry and the dynamic TFLES model provides the best comparison with the experimental data. Since the VOLVO data base is used in various benchmarking exercises [7], this paper suggests that these three elements (precise chemistry description, dynamic parameter-free turbulent combustion model and high-order numerical methods) play important roles and must be considered carefully in any LES approach.

¹CERFACS, 42 Avenue Gaspard Coriolis, 31057 Toulouse, Cedex 1, France

²Safran Helicopter Engines, 64511 Bordes, France

³Safran Aircraft Engines, Rond-point Rene Ravaut, 77550 Moissy-Cramayel, France

⁴Laboratoire EM2C, CNRS, CentraleSupélec, Université Paris-Saclay, Grande Voie des Vignes, Châtenay-Malabry cedex 92295, France

⁵CNRS, IMFT, 1 Allée du Professeur Camille Soula, 31400 Toulouse, Cedex, France

1. Introduction

The quest for a universal turbulent combustion model has been going on for a long time [8–11] but it has become more challenging in the last years. Today, turbulent combustion models are not only expected to provide reasonable estimates of mean heat release or temperature fields but also additional targets such as (1) pollutant emissions (NO_x and CO for example) as well as soot, (2) possible combustion instabilities and noise level, (3) ignition and quenching phenomena. All these objectives must be satisfied for (4) liquid fuels, and (5) the detailed chemistry characteristics of real fuels must be included.

To satisfy these five objectives, the introduction of Large Eddy Simulation (LES) has offered a powerful approach [11–14] not because the subgrid LES models are better than their classical Reynolds Averaged (RANS) counterparts but because they are applied to a more limited part of the turbulence spectrum, while the rest of the unsteady activity is directly captured by the simulation. LES applied to combustion permits a better identification, at resolved scales, of the intermittency between fresh and burnt gases regions (where properties of turbulence, pollutant emissions, etc., are different) than RANS. What the last ten years have shown however, is that LES was only part of the solution. Many other ingredients remain necessary both on the physical and the numerical aspects to make LES predictive.

There are a few usual test cases for LES of reacting flows. For turbulent swirling flames, the PRECCINSTA chamber of DLR [15] has been computed many times [3, 16–20]. Since PRECCINSTA is a swirled flame, many authors have preferred started validations with an unswirled configuration and the so-called 'VOLVO' turbulent flame [21–23] has been used as a benchmark for turbulent combustion codes for a long time [7, 24, 25] for steady flames as well as for combustion instabilities [24]. Multiple solvers were applied for the VOLVO flames, leading to results which were all different [7] showing the lack of maturity of LES for turbulent flames. Considering that the VOLVO flames are fully

premixed, gaseous flames, this indicates that major efforts are still required to address real flames such as those found in gas turbines for example.

The reasons why large discrepancies are observed for the VOLVO flames are not clear yet. Most solvers provide consistent, similar results for the cold flow in this setup, matching experimental data and demonstrating that the difficulties begin with combustion. Understanding which parts of the numerical strategy control the quality of the solution with combustion is a first but difficult step. Multiple potential sources of differences may be listed: (A) chemistry description, (B) flame / turbulence interaction model, (C) quality of the numerical solver, (D) boundary conditions, especially impedances at inlet and outlet which control the intensity of thermoacoustic modes, (E) wall numerical treatments, (F) wall temperatures and heat losses. The present work focuses on the first three sources (A) chemistry, (B) flame turbulence SGS models and (C) numerics.

Even if turbulent premixed flames can often be treated as thin interfaces, knowing whether the dynamics of these interfaces (response to small scale turbulence, to strain, to curvature) is really captured correctly for a given chemical scheme remains a daunting question for the LES community. Moreover, since objective (1) in real flames is to correctly capture all important species, LES chemical models must include more and more chemistry details. Knowing how the LES solution changes when a reasonably complex chemical scheme is used instead of a heuristic one or two-step scheme is the first objective of the present work. This objective is similar to the recent work of Zettervall et al [25]. Note that it depends not only on the chemical scheme but also on the flame/turbulence interaction model (B) used in the LES. Here the TFLES (Thickened Flame model) is retained with either an usual non-dynamic (called static in the following) or a dynamic subgrid scale formulation. The third source (C) influencing the quality of LES results is the quality of the solver itself. This question is rarely discussed in the combustion community but is central in the aerodynamics community where the search for high-order methods has driven research for a long time. In the present study, a second and a third/fourth order

method (space accuracy ⁶) are compared: results show that turbulent structures and therefore the whole flame structure are indeed sensitive to the spatial accuracy of the solver, thereby explaining why different LES solvers often lead to different results even when all physical models are the same.

Of course, the three modeling sources affecting LES studied here (A-chemistry, B-SGS turbulent combustion model and C-numeric) are not the only ones controlling the quality of LES results. The present paper aims only at demonstrating that these three are important and that the quality of LES solutions cannot be investigated if these aspects are not properly considered.

The paper is organized as follows. First the description of propane-air chemistry (a two-step global scheme and the ARC formulation proposed by Pepiot et al [1, 27, 28]) is presented in Section 2. Then, the two formulations, static and dynamic, of the TFLES model are described (Section 3). The numerical solver itself is presented in Section 4. Section 5 provides a description of the VOLVO setup and the stable combustion case retained for computations. Finally, Section 6 presents results, evidencing the influence of the subgrid scale model, the chemistry model and the solver spatial accuracy.

⁶The TTGC scheme used here [26] is fourth order accurate on regular unstructured grids and third order on arbitrary grids.

2. Chemistry description

In most turbulent flames, chemistry description can rapidly become an issue. The Volvo experiment is a usual benchmark for codes which ultimately will have to handle kerosene flames. Even if simplified chemical schemes (one or two steps) can be used for the premixed propane/air flames of the Volvo rig, going to more precise chemical schemes has become a necessity: today such options are readily maturing and for example, Analytically Reduced Chemistry (ARC) tools can produce chemical schemes that LES can fully resolve [27, 28]. Here, two chemical schemes have been used to describe propane-air flames.

2.1. A two-step scheme for propane-air flames

The first scheme is a two-step scheme based on a fast oxydation reaction followed by a CO-CO₂ equilibrium. Six species are taken into account (C_3H_8 , O_2 , CO_2 , CO , H_2O and N_2) and two reactions [24]:



The reaction rates q_j follow an Arrhenius law:

$$q_1 = A_1 \left(\frac{\rho Y_{C_3H_8}}{W_{C_3H_8}} \right)^{0.9028} \left(\frac{\rho Y_{O_2}}{W_{O_2}} \right)^{0.6855} \exp \left(\frac{-E_{a,1}}{RT} \right) \quad (3)$$

$$q_2 = A_2 \left[\left(\frac{\rho Y_{CO}}{W_{CO}} \right)^{1.0} \left(\frac{\rho Y_{O_2}}{W_{O_2}} \right)^{0.5} - \frac{1}{K} \left(\frac{\rho Y_{CO_2}}{W_{CO_2}} \right)^{1.07} \right] \exp \left(\frac{-E_{a,2}}{RT} \right) \quad (4)$$

The pre-exponential constants A_j and the activation energies E_j are given in Table 1, and K is the equilibrium constant [29].

2.2. An analytically reduced scheme (22 species) for propane-air flames

The second method is based on the ARC approach. Using YARC reduction tools [1], the ARC chemical scheme is constructed from a skeletal mechanism

	$A_j[\text{cgs}]$	$E_j[\text{cgs}]$
Reaction 1	2.0×10^{12}	3.3×10^4
Reaction 2	-4.51×10^{10}	1.2×10^4

Table 1: Two-step reduced chemical mechanism for $C_3H_8 - Air$. Pre-exponential factor A_j and activation energies E_j are both in *cgs* units [24].

proposed by Jerzembeck [30] using 99 transported species and 669 reactions. This skeletal scheme was derived from the LLNL detailed mechanisms for n-heptane [31] and iso-octane [32]. Laminar flames with an equivalence ratio in the range $\phi = 0.5 - 1.6$ are chosen as the sampled reference cases for the reduction process. The first step of the methodology is to discriminate unimportant species and reactions using the directed relation graph method with error propagation [33]. Then, suitable species for Quasi-Steady State Approximation (QSSA) are selected using the Level Of Importance criterion [34]. The resulting ARC chemical scheme (named ARC-22-12QSS in the following) treats 22 transported species and 12 QSS species (Table 2).

Transported species (22)	QSS species (12)
N2, O, O2, H, OH	CH2GSG-CH2, CH3O, C2H5, HCO, HCCO
H2, H2O, H2O2, HO2, CO	C2H3, CH2CHO, C3H5-A-C3H5, I-C3H7, N-C3H7
CH2O, CH3, C2H6, CH4, C2H4	I-C3H7O2, N-C3H7O2
CO2, CH3O2, CH3O2H, C2H2, C3H6	
C3H5O, C3H8	

Table 2: Summary of *ARC - 22 - 12QSS*: transported (left) and Quasi Steady State (QSS) (right) species.

2.3. Comparison of two-step and ARC schemes on premixed laminar flames

Since the VOLVO experiment is fully premixed, a good method to compare chemical schemes is to apply them for premixed laminar flames. This is done

here in terms of flame speeds and response to strain at atmospheric pressure. Adiabatic flame temperatures are not presented because they match very well for both schemes. The two-step and ARC schemes are validated against the Jerzembeck skeletal mechanism [30] in Fig. 1. Flame speeds are computed using Cantera for a 1D resolved planar flame, at the operating conditions used for the LES simulations ($T_0 = 288K$ and $P_0 = 101325Pa$): results show a good agreement for the ARC scheme and a slight overestimation of the flame speed for the two-step reduced chemistry.

Flame response to stretch was also studied using 1D premixed counter-flow flames computed with Cantera. Premixed fresh gases are injected on one side and burnt gases at the adiabatic flame temperature on the other. For consistency with the counter-flow configuration where the flame is stabilized on a stagnation plane, the consumption speed S_c is retained to study the flame response to stretch. Fig. 2 shows that the ARC mechanism captures stretch effects as well as the full scheme while the two-step mechanism overestimates them.

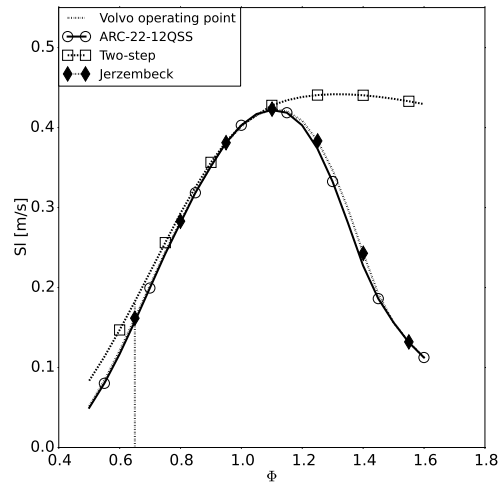


Figure 1: Comparison of Jerzembeck skeletal mechanism [30], two-step and ARC chemistry for laminar flame speed, $T_0 = 288K$, $P = 101325Pa$.

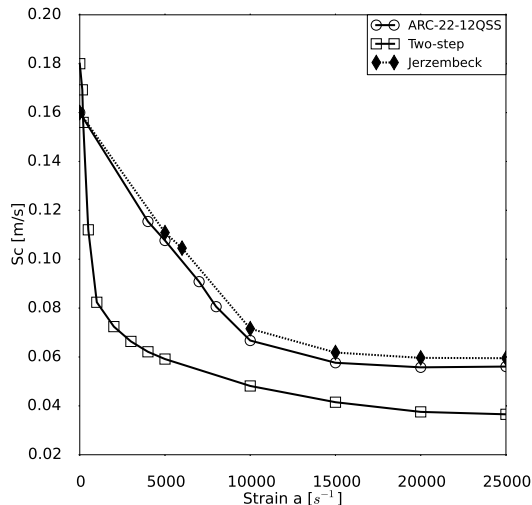


Figure 2: Comparison of Jerzembeck skeletal mechanism [30], two-step and ARC flame consumption speed response to stretch, $\Phi = 0.65$, $T_0 = 288K$ and $P = 101325Pa$.

3. The TFLES model for flame/turbulence SGS interactions

Using a precise chemical scheme is only part of the solution in a LES solver. Handling the subgrid scale interaction model between turbulence and flames is a second critical part. This question has been central in the RANS community for decades [35–37] and it would be a mistake to believe that it can simply be ignored in LES codes: the interaction between turbulence and flames must be modeled. The first reason for this is that flame fronts are usually too thin to be resolved even on LES grids and a model is required to handle this difficulty. Discussing all possible models for SGS in combustion is beyond the objectives of this paper. However it is worth mentioning that the constraint of using complex chemical schemes with multiple independent species strongly limits possible choices for turbulent combustion models. Tabulation techniques for example, which assume frozen flamelet structures and have been very successful in the past [38, 39], probably reach their limits here because they constrain the chemical state to a manifold of limited dimension (2 or 3). Similarly, using pdf

methods [40] becomes difficult: with ARC chemistry for the present C_3H_8 -air flames, 22 independent species are used leading to a pdf space of dimension 223 (with temperature). In the present study, the TFLES (Thickened Flame) model has been used. This model explicitly solves conservation equations for all species considered in the chemical scheme, thickening their spatial structure to allow its resolution on the numerical grid and accounting for subgrid scale thickening effects through an efficiency function based on DNS. Therefore it is compatible with complex schemes such as ARC as described in the previous section.

A second characteristic of turbulent combustion models is that they all rely on a few constants which are often adjusted by the user to match the overall flame structure. This is true also for the standard static TFLES models where a β constant is user specified in the expression of the subgrid efficiency. In the present work, we propose to move to a fully dynamic model [2, 3, 41–44] where no user-adjustable coefficient exists anymore. The standard TFLES model is described in Section 3.1 while the dynamic formulation is summarized in Section 3.2.

3.1. Static TFLES model

In the TFLES model, flames are artificially thickened to be resolved on the numerical mesh, without modifying their flame speeds [4, 26, 45–48]. The thickening process is done by multiplying diffusion terms and dividing reaction rates by a local thickening factor F . Since a thickened flame is less sensitive to turbulence, an efficiency function is introduced to compensate the corresponding reduction of flame surface [4, 26]. Multiple expressions can be found in the literature for an efficiency function Ξ_Δ which corresponds to the SGS flame/turbulence interaction model: Ξ_Δ is expressed as the ratio between the total flame front wrinkling, and its resolved part. It depends on the mesh size Δ and the subgrid scale velocity u'_Δ . The transport equations for the filtered

species mass fractions \tilde{Y}_k are written:

$$\begin{aligned} \frac{\partial \bar{\rho} \tilde{Y}_k}{\partial t} + \frac{\partial}{\partial x_j} (\bar{\rho} \tilde{u}_j \tilde{Y}_k) &= \frac{\partial}{\partial x_j} \left[\left(\Xi_{\Delta} F \frac{\mu}{S_{c,k}} + (1-S) \frac{\mu_t}{S_{c,k}^t} \right) \frac{W_k}{W} \frac{\partial \tilde{X}_k}{\partial x_j} - \bar{\rho} \tilde{Y}_k (\tilde{V}_j^c + \tilde{V}_j^{c,t}) \right] \\ &+ \frac{\Xi_{\Delta}}{F} \dot{\omega}_k (\tilde{Y}_k, \tilde{T}), \end{aligned} \quad (5)$$

where ρ is the density, u the velocity vector, X_k and W_k the mole fraction and atomic weight of species k , $S_{c,k}$ and $S_{c,k}^t$ the Schmidt and turbulent Schmidt numbers. μ and μ_t are the laminar and turbulent dynamic viscosities. The sigma model [49] is used to model the sub-grid turbulent kinematic viscosity. The local thickening factor F is applied to the flame front thanks to a sensor S which depends on the local temperature and mass fractions. S is unity in the flame zones where thickening is applied. $\dot{\omega}_k$ is the reaction rate of species k , estimated from Arrhenius laws. The Reynolds spatial filtering operation is indicated with the operator $\bar{\cdot}$, while $\tilde{\cdot}$ denotes the mass-weighted (Favre) spatial filtering. The following relation for the correction diffusion velocities is used:

$$\tilde{V}_j^c + \tilde{V}_j^{c,t} = \sum_{k=1}^N \left(\Xi_{\Delta} F \frac{\mu}{\bar{\rho} S_{c,k}} + (1-S) \frac{\mu_t}{\bar{\rho} S_{c,k}^t} \right) \frac{W_k}{W} \frac{\partial \tilde{X}_k}{\partial x_j}. \quad (6)$$

The turbulent combustion model is also applied to the filtered total energy conservation equation \tilde{E} :

$$\begin{aligned} \frac{\partial \bar{\rho} \tilde{E}}{\partial t} + \frac{\partial}{\partial x_j} (\bar{\rho} \tilde{u}_j \tilde{E}) &= - \frac{\partial}{\partial x_j} [\tilde{u}_i \bar{P} \delta_{ij} - \tilde{u}_i \bar{\tau}_{ij}] \\ &+ \frac{\partial}{\partial x_j} \left[C_p \left(\Xi_{\Delta} F \frac{\mu}{P_r} + (1-S) \frac{\mu_t}{P_r^t} \right) \frac{\partial \tilde{T}}{\partial x_j} \right] \\ &+ \frac{\partial}{\partial x_j} \left[\sum_{k=1}^N \left(\left[\Xi_{\Delta} F \frac{\mu}{S_{c,k}} + (1-S) \frac{\mu_t}{S_{c,k}^t} \right] \frac{W_k}{W} \frac{\partial \tilde{X}_k}{\partial x_j} - \bar{\rho} \tilde{Y}_k (\tilde{V}_j^c + \tilde{V}_j^{c,t}) \right) \tilde{h}_{s,k} \right] \\ &+ \frac{\Xi_{\Delta} \dot{\omega}_T (\tilde{Y}_k, \tilde{T})}{F}, \end{aligned} \quad (7)$$

where \bar{P} is the filtered pressure field, C_p the mass heat capacity at constant

pressure, $\tilde{h}_{s,k}$ the sensible enthalpy of species k , $\bar{\tau}$ the filtered viscous stress tensor, P_r and P_r^t the Prandtl and turbulent Prandtl numbers, and $\dot{\omega}_T$ the heat release rate. Eqs. 5 and 7 propagate a flame front of thickness $F\delta_L^0$ with the velocity $S_t = \Xi_\Delta S_L$, where δ_L^0 is the laminar flame thickness. The thickening factor F can be adjusted to ensure that the grid is sufficient to resolve the thickened flame front. Typically F is chosen such that $F\delta_L^0/\Delta$ is of the order of 7 (7 points to resolve the flame structure).

In the current work, two TFLES models were tested, the usual Charlette model [4], and the Charlette dynamic model [3, 41, 43, 46, 50]. Both introduce SGS flame front wrinkling thanks to the efficiency function Ξ_Δ . The usual Charlette model, estimates Ξ_Δ from an algebraic expression derived assuming an equilibrium between turbulence motions and flame front wrinkling [4, 42]:

$$\Xi_\Delta^{Ch} \left(\frac{\Delta}{\delta_L^0}, \frac{u'_\Delta}{S_L}, Re_\Delta \right) = \left(1 + \min \left[\max \left(\frac{\Delta}{\delta_L^0} - 1, 0 \right), \Gamma_{Ch} \left(\frac{\Delta}{\delta_L^0}, \frac{u'_\Delta}{S_L}, Re_\Delta \right) \frac{u'_\Delta}{S_L} \right] \right)^{\beta_{Ch}}, \quad (8)$$

where Γ_{Ch} is a function derived from DNS of flame-vortex interactions. It measures the ability of vortices to effectively wrinkle the flame front and create flame area. β_{Ch} is the unique user-defined parameter which is of the order of 0.5 for most flames. u'_Δ and $Re_\Delta = u'_\Delta \Delta / \nu$ are the subgrid scale turbulent velocity and Reynolds number, respectively, ν being the fresh gas kinematic viscosity. u'_Δ is calculated using an operator based on the rotational of the velocity field to remove the dilatational part of the velocity [26].

3.2. Dynamic TFLES formulation

When u'_Δ/S_L is large, Eq. 8 degenerates to [51, 52]:

$$\Xi_\Delta = \left(\frac{\Delta}{\delta_L^0} \right)^\beta, \quad (9)$$

which is the well-known expression of total area in fractal surfaces of dimension $D = \beta + 2$ [51, 52]. Eq. 9 simply states that the SGS surface has a fractal dimension $\beta + 2$, an inner cutoff set to the laminar flame thickness δ_L^0 [4] and

an outer cutoff Δ (the grid size). Eq. 9 relies on a coefficient β specified by the user. This raises two difficulties: (1) β is often unknown and (2) β may change with location and time. Tests in LES of explosions [53] or flames in internal combustion engines [43, 54] for example show that β should be a function of space and time, and that different β values have to be used when the Reynolds number varies over a wide range. Developments of turbulent combustion models [2, 3, 41] show that a proper solution to this limitation is to make the turbulent combustion model for Ξ_Δ dynamic as done for dynamic models for the SGS transport terms [55–58]. With the dynamic wrinkling formulation, the exponent β of Eq. 9, is automatically adjusted from the resolved progress variable (\tilde{c}) field. This is done by equating the flame surface densities computed at filtered and test-filtered level (Germano-like identity [56]):

$$\langle \widehat{\Xi_\Delta |\nabla \tilde{c}|} \rangle = \langle \Xi_{\gamma\Delta} |\nabla \tilde{c}| \rangle, \quad (10)$$

where c is the progress variable, estimated here from the temperature. The $\widehat{\cdot}$ symbol denotes the test-filtering operation, and $\langle \cdot \rangle$ denotes an averaging operator [46] that can be the overall computational domain (dynamic global formulation) or a small local volume (dynamic local formulation). In this latter case, the averaging operation can be replaced by a Gaussian filtering of size Δ_{avg} [41, 59]. The ratio γ between the effective filtered scale (i.e the scale of the filter that should be applied to the instantaneous field to have the same result as the one computed using the successive combination of both LES and test filters) and the LES filtered scale is given by:

$$\gamma = \sqrt{1 + \left(\frac{\widehat{\Delta}}{\Delta}\right)^2}. \quad (11)$$

Combining Eqs 9 and 10, and assuming that β is constant over the averaging domain $\langle \cdot \rangle$ provides the value of β :

$$\beta = \frac{\log \left(\langle \widehat{|\nabla \tilde{c}|} \rangle / \langle |\nabla \tilde{c}| \rangle \right)}{\log(\gamma)}. \quad (12)$$

In this work, only the local formulation was used for the dynamic model: β is computed at each point of the mesh.

4. Second and third-order LES solvers

An additional component of LES lies in the numerical schemes adopted by the CFD solver. Different numerical strategies are possible to solve the set of modeled LES equations. These numerical schemes can be either explicit or implicit, the effective difference being the size of the time-step accessible to the numerical integrator without going unstable or affecting the actual flow reference time scales targeted by the simulation. Implicit solvers are often advocated although this choice may induce difficulties in the parallelization of the algorithms and their efficiency with increasing numbers of processors. Furthermore, arbitrarily imposing a time step several orders of magnitudes higher than the smallest cell size to flow speed ratio naturally raises precision issues and comes with undesirable dispersive/dissipative properties of the solver which can overshadow the modeling. In the following, only fully compressible explicit schemes are tested: (a) the Lax-Wendroff scheme [6] (LW) which is second order in time and space and (b) the TTGC scheme [5] which offers third order accuracy in time and space on arbitrary unstructured meshes. For a typical CFL condition of 0.1 (based on the local mesh characteristic size and acoustic wave speed which involves the flow speed and sound velocity), these schemes have very distinct spectral features as evidenced by Fig. 3 which shows the amplification factor ((a) its norm and (b) its phase) of each scheme for a 1D convection problem. For high wavelengths that can be captured by a reasonable number of points ($0 < k\Delta < 1$ where k stands for the wave number), the signal can be transported without too much numerical dissipation, Fig. 3(a), and at the correct speed, Fig. 3(b). Differences start however appearing for both properties around $k\Delta \approx 1$. For shorter wavelengths or equivalently larger non-dimensional wave numbers, two distinct behaviors are clearly shown. Beyond $k\Delta \approx 1$, TTGC is clearly superior both in terms of dissipation and dispersion. This implies that the TTGC

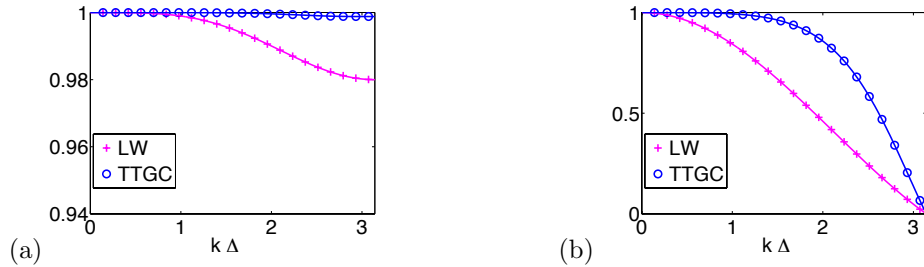


Figure 3: Amplification function of the Lax-Wendroff and TTGC schemes for a CFL number of 0.1: (a) modulus of the amplification function and (b) relative phase velocity as a function of the non-dimensional wave number $k\Delta$.

scheme can preserve the small-scale structures generated in high shear regions better than LW for the same grid resolution. Note that these structures may be of potential importance at the flame front because they are the source of flame wrinkling. This can be even more critical with complex chemical schemes where multiple chemical scales are present and the response of the flame to the flow structures can be of importance. For the same reason, the generation of flow instabilities will be impacted by the numerical scheme as linearly unstable modes may grow or be damped depending on the grid resolution and equivalently the scheme properties. This specific difficulty is illustrated in Fig. 4 for the growth of a spatial perturbation of wavelength λ by a piecewise continuous velocity deficit noted ΔU . Solved analytically by Rayleigh [60], this problem can be resolved numerically for numerical scheme assessment. Fig. 4(b) presents the comparison between theory, TTGC and LW. For all simulations, the grid is $2D$, uniform, made of square cells of size $\Delta = 8$ mm. d corresponds to the length of the velocity ramp between U_1 and U_2 (here $d = 0.1$ m). Only the axial length α (Fig. 4(a)) of the computational domain is changed and matches the initial perturbation wavelength λ . This results in a fixed axial spacing to wavelength ratio, the problem being resolved for thirty different values of the wavelength λ covering the range $[0.3 - 2.5$ m].

For large wavelength perturbations (low values of d/λ) both schemes per-

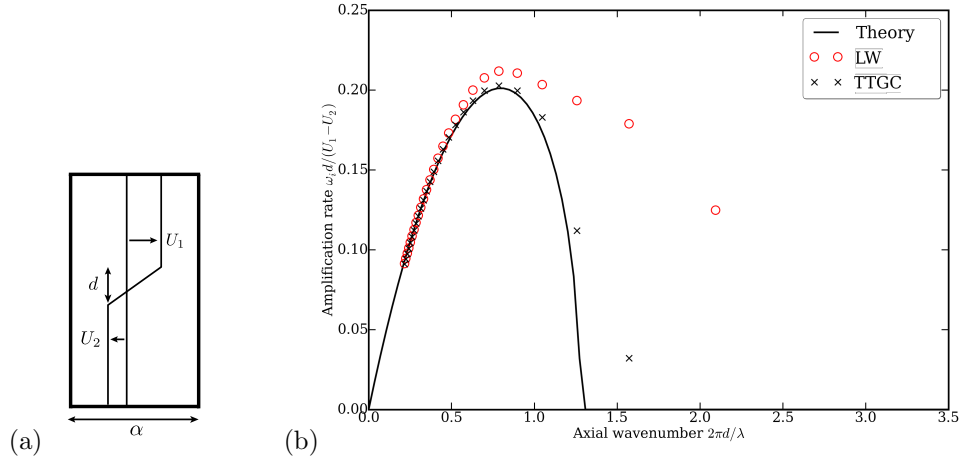


Figure 4: (a): Schematic of the numerical case to study the growth of a perturbation superimposed onto an inviscid piecewise linear velocity field of thickness d . (b): Non-dimensional growth rate, $\omega_i d / (\Delta U)$, of a perturbation using TTGC or LW for a CFL condition of 0.7.

form well. Beyond $\frac{2\pi d}{\lambda} = 0.8$, however, the LW scheme greatly overestimates the linear growth rate of the perturbation while TTGC is much closer to the analytical solution. Again, this suggests that high order schemes are better suited to LES of reacting shear flows.

5. The VOLVO experiment

5.1. Experimental configuration

The VOLVO combustor [21–23] (Fig. 5) is a straight rectangular cross-section channel (0.12 m x 0.24 m), divided into an inlet section, and a combustor section ending into a round exhaust. The total length of the configuration (without exhaust) is 1.55 m.

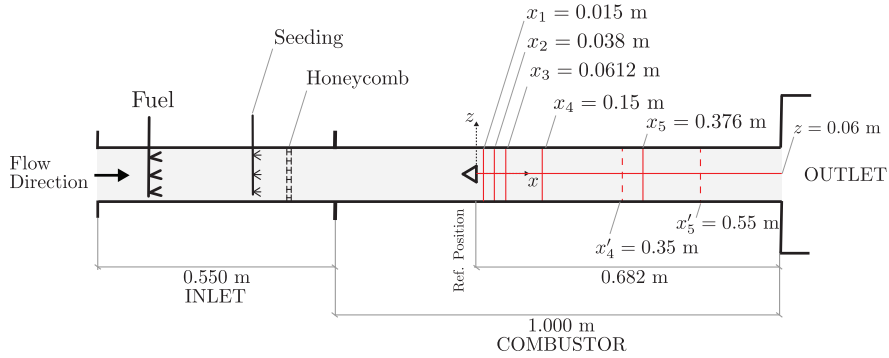


Figure 5: *The VOLVO rig combustor. The computational domain is identified by the shaded area.*

Gaseous propane is injected and premixed with air in the inlet section, upstream of a honeycomb used to control the turbulence level. Three bluff-body flameholders were used during the experimental tests, but only the equilateral triangular-shaped one of height $h = 0.04$ m is studied in the current work. The top and bottom walls of the combustor are water-cooled and the side walls are air-cooled in order to accommodate the quartz windows for optical access. Experimental data, including high-speed and Schlieren imaging, gas analysis, Laser Doppler Velocimetry (LDV), and Coherent Anti-Stokes Raman Scattering (CARS), are used to investigate a baseline case described in Table 3. For the operating point used in the present work, only velocity and turbulence data are available. We will also compare mean and RMS temperature profiles but note that these data were obtained experimentally at slightly different operating points (Table 3). Measurements were made on seven longitudinal ($x_1, x_2, x_3, x_4, x'_4, x'_5$ and x_5) and one (z) transverse locations (Fig. 5).

Publications	ϕ	U_{bulk} (m/s)	T_0 (K)	Re	Comment
Sjunnesson et al. [23]	0.65	16.6	288	48000	Measurements: T and Y_{CO}
Sjunnesson et al. [21]	0.65	17.3	288	47000	Measurements: U , U_{rms} , V and V_{rms}
Sjunnesson et al. [22]	0.61	17.3	288	47000	Measurements: T and T_{rms}
Zettervall et al. [25]	0.62	17.6	288	46592	LES: U , V , V_{rms} , T , T_{rms} , Y_{CO}
Present work	0.65	17.3	288	47000	LES: U , V , U_{rms} , V_{rms} , T and T_{rms}

Table 3: Comparison between the operating point used in the present work and available literature measurements and operating points.

Additional cases experiencing different types of combustion instabilities also exist [24] but here, only the stable case is studied to quantify the influence of chemical schemes, turbulent combustion models and numerical schemes.

5.2. Numerical setup

LES is performed using the AVBP solver co-developed by CERFACS and IFPEN [61]. It solves the fully compressible multispecies Navier-Stokes equations on unstructured grids. The computational domain is shown in Figs. 5 and 6. In the longitudinal direction, it includes the entire burner (the inlet and combustor sections). In the transverse direction, the mesh includes exactly the chamber transverse dimension (0.24 m) and not only a slice of it as done in previous papers [62–64], to capture all large scale effects as well as transverse acoustic modes. Two elements which were not fully characterized in the experiments (fuel feeding line and honeycomb) are not considered in the simulations since their impacts on the results are marginal [24]: fully premixed gases are injected at the inlet of the LES and replace the fuel feeding line. Turbulence is injected at $x = 0$ m in the inlet plane.

The unstructured mesh comprises 68 million tetrahedral elements and is refined in shear and combustion regions (Fig. 6). The near wall region of the

flame holder features dimensionless wall distances of $y^+ = 25$, versus $y^+ = 80$ near the combustor walls.

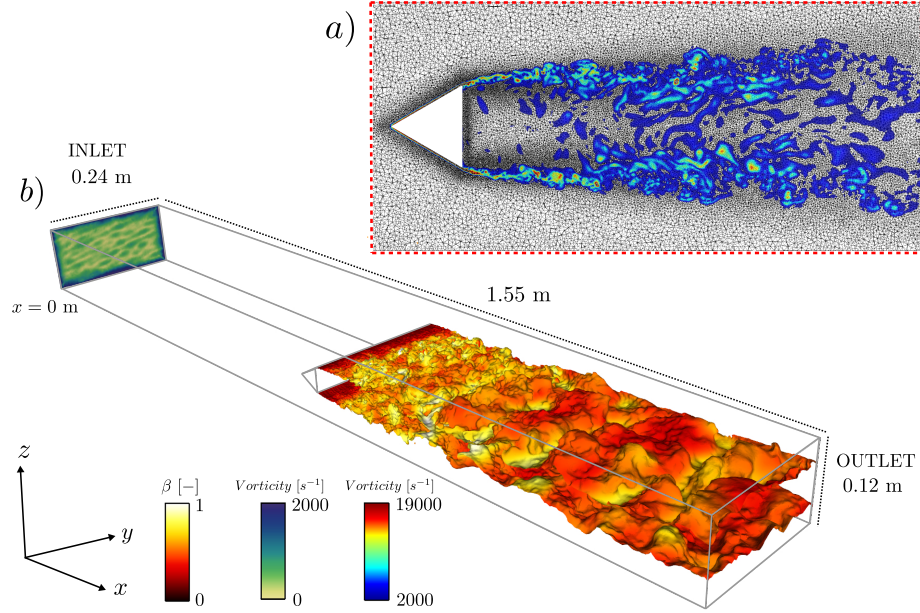


Figure 6: Overview of the computational domain, with a focus on the unstructured mesh refinement downstream of the flame holder, at $y = 0.12$ m (a). The flame is represented through an iso-surface of progress variable $c = 0.5$, colored by β of run $2s - ttgc - dyn$ (red colormap, b). The vorticity field ranging from 0 s^{-1} to 2000 s^{-1} is represented by the green colormap (inlet, b) whereas the vorticity field ranging from 2000 s^{-1} to 19000 s^{-1} is represented by the blue colormap (a).

Inlet and outlet boundary conditions are treated with Navier-Stokes Characteristic Boundary Conditions (NSCBC) [65]. To avoid exciting a particular acoustic mode, these two boundary conditions are modeled as non-reflecting sections. Turbulence is injected at the inlet using the method of Guezennec and Poinot [66]. The turbulence intensity of the inlet section is equal to 8 % of the bulk velocity and decreases at the honeycomb position to 3 %, which corresponds to measurements obtained at this position [21]. The walls are modeled as adiabatic no-slip walls. The unique closure coefficient β_{Ch} of the Charlette static formulation model is set to the standard value: $\beta_{Ch} = 0.5$. For the dy-

Simulations	Turbulent combustion model	Chemical scheme	Numerical scheme	Normalized CPU cost
2s-lw	non-dynamic formulation	two-step	LW	1
2s-ttgc-dyn	dynamic formulation	two-step	TTGC	2.5
2s-lw-dyn	dynamic formulation	two-step	LW	1.6
arc-lw-dyn	dynamic formulation	ARC-22-12QSS	LW	3.2
arc-ttgc-dyn	dynamic formulation	ARC-22-12QSS	TTGC	5.5

Table 4: Summary of simulated cases and CPU costs (normalized by the fastest computation: $2s - lw$)

dynamic formulation of Eq. 12, filter, effective filter and averaging filter widths are set to $\Delta = 1.4F\delta_L^0$, $\gamma = 2.2$ and $\Delta_{avg} = 2.5\Delta$ respectively. A calibration factor in the filter width relation (in the current work equal to 1.4), has been introduced by Wang et al. [42] in order to recover $\beta = 0$ and $\Xi_\Delta = 1$ for planar laminar flames. Results are very weakly dependent on these parameters [2].

6. Results

Table 4 summarizes the VOLVO simulated cases. All dimensions, velocities and velocity fluctuations are made dimensionless with the flameholder height, $h = 0.04$ m, and the inlet bulk velocity respectively. Only reacting results are presented. Cold flow results match the experimental data of Sjunnesson [21] very well in terms of mean and RMS values.

6.1. Influence of the turbulent combustion model

The effects of the turbulent combustion static and dynamic formulations are investigated first.

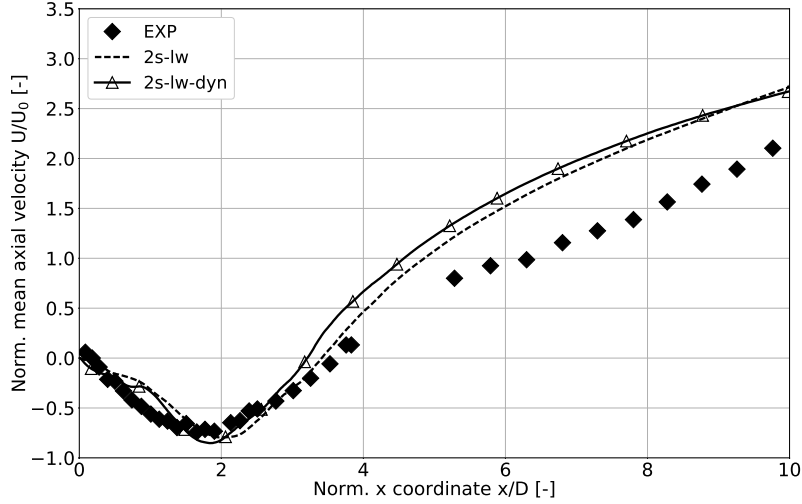


Figure 7: Mean axial velocity evolution along the central axis of the Volvo burner measured experimentally and obtained by LES with the Charlette static model ($\beta_{Ch} = 0.5$) and the Charlette dynamic model. The axis measures the downstream location from the backward wall of the bluff-body (cf. axis x at $z = 0.06$ m in Fig. 5).

Figure 7 compares the mean axial velocity profiles computed with the non-dynamic and the dynamic formulations. The dynamic approach does not have a major impact on these results. The spatial evolution of the β parameter along the flame front computed with the dynamic formulation is illustrated on Fig. 8. On the major part of the flame, β is close to $\beta_{Ch} = 0.5$, except downstream of the bluff-body and at the end of the flame, where $\beta < \beta_{Ch}$. This explains why the dynamic formulation has a limited impact on the burnt gas velocity for this case. Note that this comparison can be misleading: the dynamic model procedure determined the values of β on its own while the $\beta_{Ch} = 0.5$ value is specified by the user and can be adjusted to fit the experimental data. Going to a dynamic formulation removes one user-specified constant and significantly increases the prediction capacities of the model.

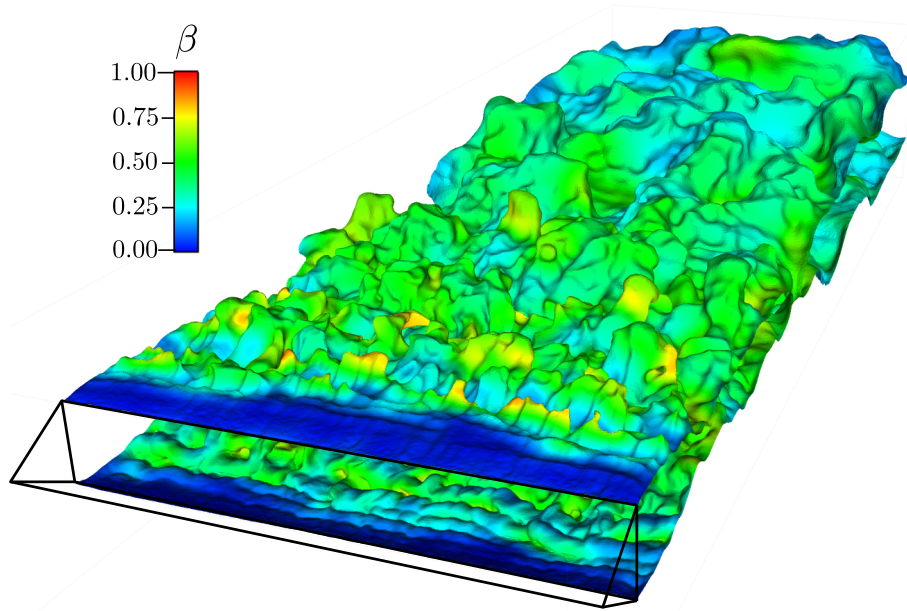


Figure 8: Iso-surface of the progress variable $c = 0.5$, colored by the β parameter computed with the dynamic formulation (case $2s - lw - dyn$).

Figure 9 top provides a scatter plot view for all points in the chamber of the thickening factor F conditioned by heat release as a function of the local temperature-based progress variable c for two cases: $2s - lw - dyn$ (triangles), and a 1D resolved laminar premixed flame computation (black line). The maximum F values are obtained either in highly reacting points or in places where the mesh is not very fine. F never exceeds 30 and most points have F values of the order of 5 to 10. Figure 9 bottom displays a scatter plot of the fuel reaction rate as a function of the progress variable. As expected, compared to the laminar flame (solid line), the reaction rate is reduced by a factor F due to the thickening procedure.

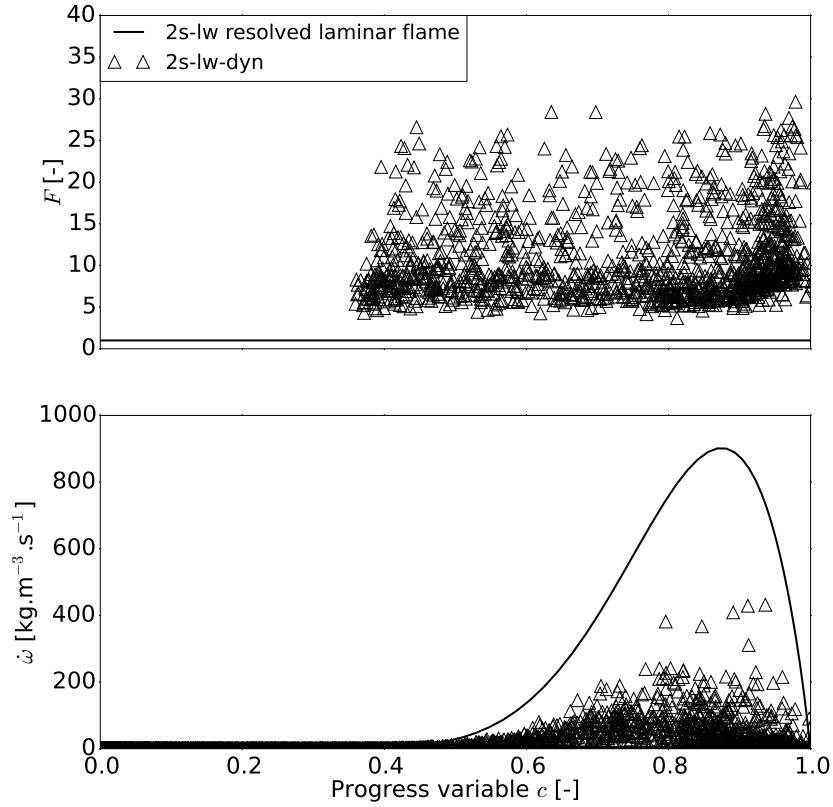


Figure 9: Scatter plot of the thickening factor F conditioned by heat release (top) and the fuel reaction rate (bottom) as a function of the temperature-based progress variable c . The black line corresponds to a 1D resolved unthickened laminar premixed flame computed at $\phi = 0.65$, $T_0 = 288K$ and $P_0 = 101325Pa$ (case 2s - lw - dyn).

The PDF of β over the whole domain is given in Fig. 10. The value $\beta = 0.5$ used for the static model belongs to the range predicted by the dynamic model but is not the most probable value.

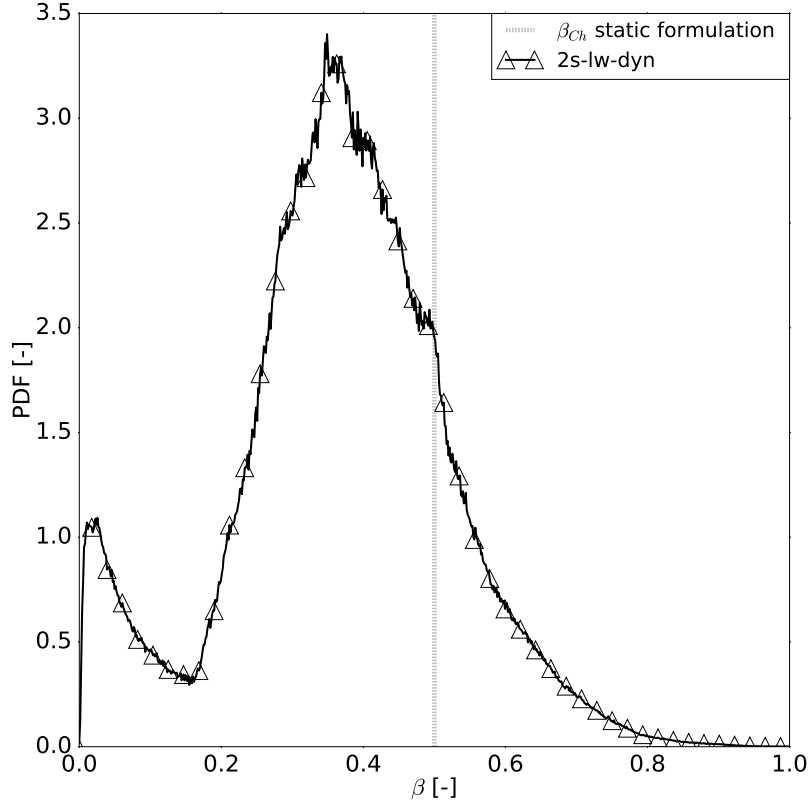


Figure 10: *PDF of the wrinkling exponent β (12) computed along the flame front, for a progress variable ranging between $0.4 \leq \tilde{c} \leq 0.99$ (in practice for $\tilde{c} \leq 0.4$, $\dot{\omega} \approx 0$, cf. Fig. 9).*

6.2. Influence of chemistry description and numerical scheme

The influence of chemistry description and numerical scheme on LES predictions are investigated together in this section. The two chemical schemes (two-step and ARC-22-12QSS) and the two numerical schemes (LW and TTGC) are tested, all with the dynamic turbulent combustion model.

Figure 11 compares the axial profiles of the mean axial velocity component.

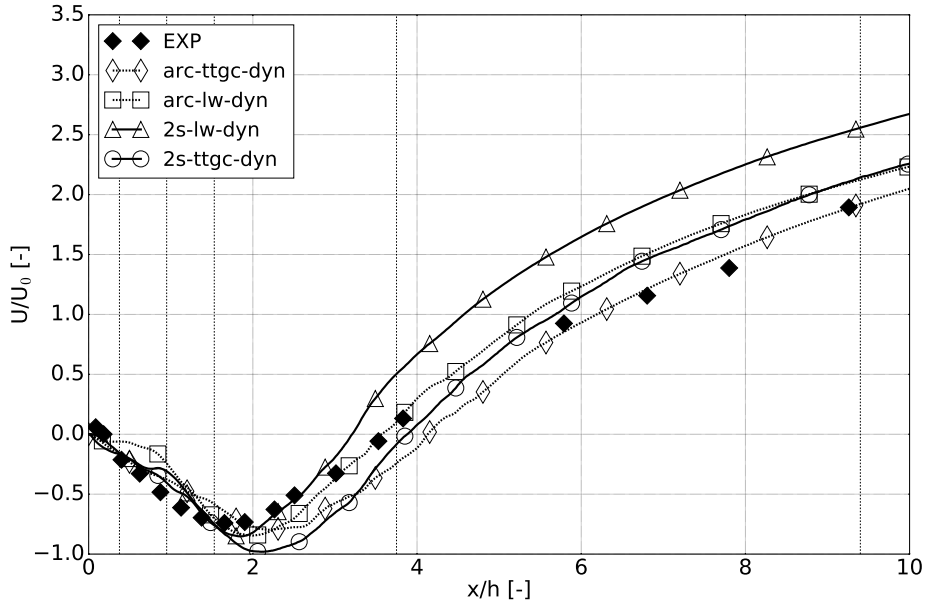


Figure 11: Mean axial velocity evolution along the central axis of the Volvo burner measured experimentally and obtained with LES for arc-lw-dyn, arc-ttgc-dyn, 2s-lw-dyn and 2s-ttgc-dyn (see Table 4 for runs description). All cases are computed with the Charlette dynamic model. The axis measures the downstream location from the backward wall of the bluff-body (cf. axis x at $z = 0.06$ m in Fig. 5).

The mean recirculation zone amplitude is correctly predicted for all cases but its length increases with TTGC. This growth may be due to a longitudinal low-frequency oscillation that would require a tuning of the inlet and outlet impedances in the LES. The best results are obtained with the combination of ARC chemistry and TTGC numerical scheme, which is not surprising since the chemical description is closer to the real mechanism and the numerical scheme accuracy is higher in time and space. Moreover, the flame response to stretch is better reproduced with ARC, as shown in Fig. 2. Figure 12 compares PDFs of the tangential strain calculated along the flame front, for a filtered progress variable ranging between $0.4 \leq \tilde{c} \leq 0.99$. Note that, to be consistent with results in Fig. 2, the contribution of flame front curvature effects on stretch is not taken into account. All flame fronts are subject to a tangential strain smaller than

$2000s^{-1}$, which corresponds to the range where a significant difference exists between ARC and two-step laminar consumption speed (Fig. 2). This could influence the width of mean transverse temperature profiles.

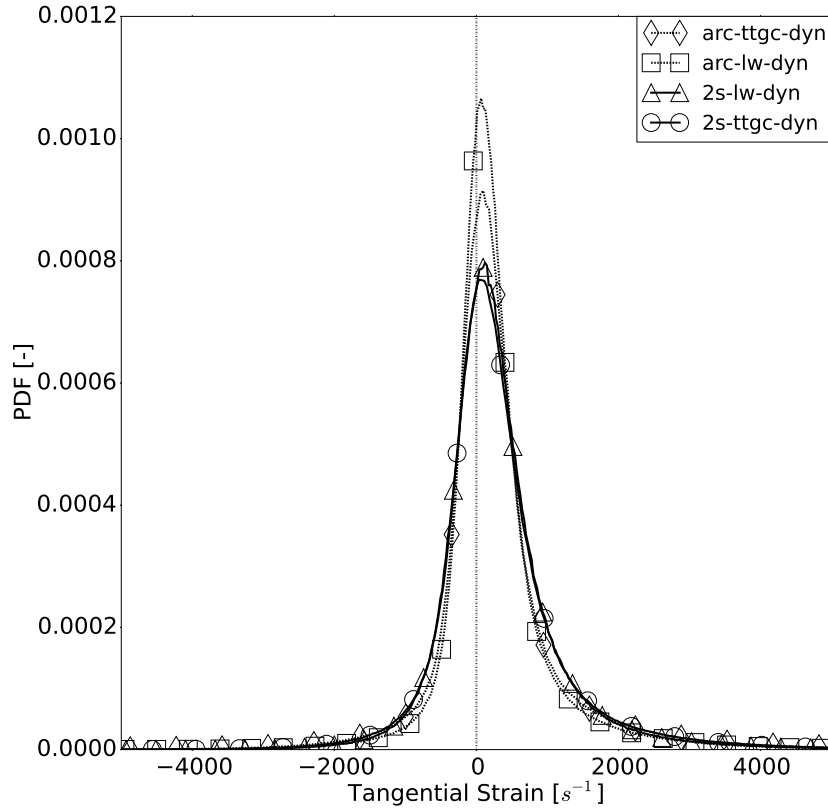


Figure 12: *PDF of tangential strain computed along the flame front, for a filtered progress variable ranging between $0.4 \leq \bar{c} \leq 0.99$.*

Figure 13 presents transverse profiles of the mean normalized axial velocity component. For all cases the first three profiles (x_1 to x_3) located in the recirculation zone are well predicted. Differences are observed on x_4 and x_5 profiles in the burnt gas acceleration zone ($2 < x/h < 9$ in Fig. 11). Except for *arc-ttgc-dyn* which provides again the best results, the mean axial velocity

at planes x_4 and x_5 is also overestimated for all other simulations, indicating that combustion is too fast with these models.

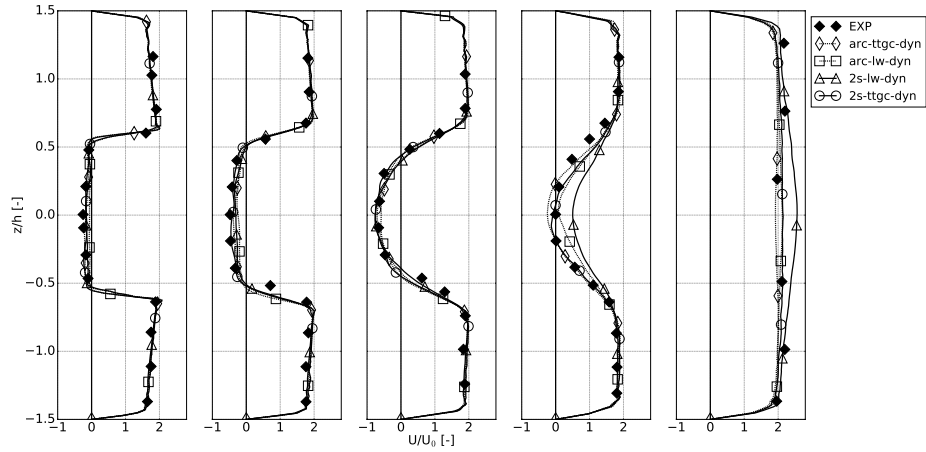


Figure 13: *Transverse profiles of mean normalized axial velocity at measurement planes $x_1 - x_5$ of Fig. 5.*

Figure 14 compares transverse profiles of the normalized RMS axial velocity fluctuations U_{rms} from x_1 to x_5 : U_{rms} is reasonably well captured by all LES (note that only RMS fluctuations of the resolved field are considered). Figure 15 shows that the primary factor controlling RMS transverse velocity profiles is the chemical scheme: indeed, V_{rms} profiles computed using the ARC chemical scheme are in good agreement with experimental data, which is not the case with the two-step mechanism.

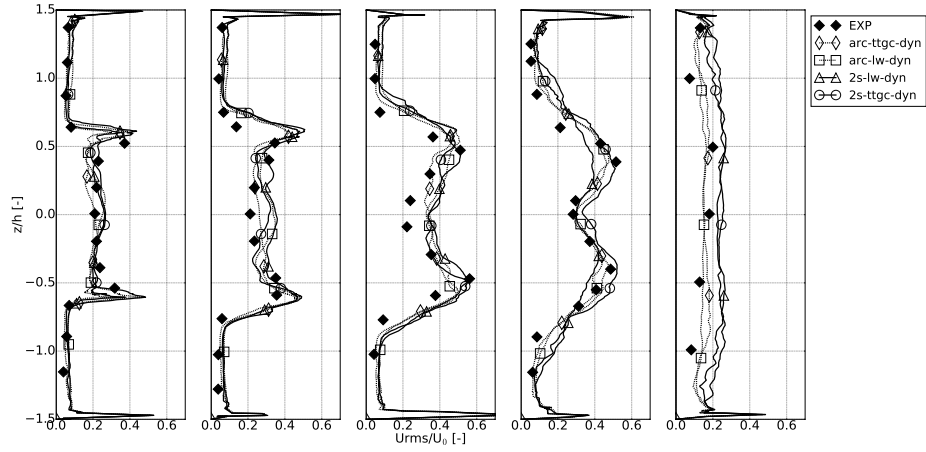


Figure 14: Transverse profiles of the normalized RMS axial velocity component at measurement planes $x_1 - x_5$ on Fig. 5.

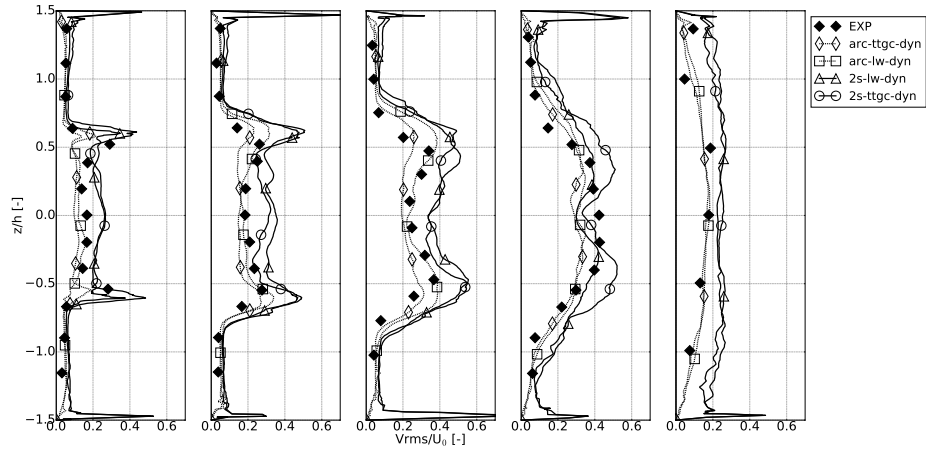


Figure 15: Mean transverse profiles of the normalized RMS transverse velocity component at measurement planes $x_1 - x_5$ on Fig. 5.

Figure 16 shows the transverse profiles of the normalized mean temperature. The broadening of the experimental profiles is slightly more pronounced than in the LES. This could result from a lack of turbulent mixing between low and high temperature regions or to a difference in the flame front location. This latter one is more probable since experimental temperature measurements were made with a bulk velocity $U_{bulk} = 16.6 \text{ m/s}$, which is slightly lower than the

one used in all LES runs (Table 3).

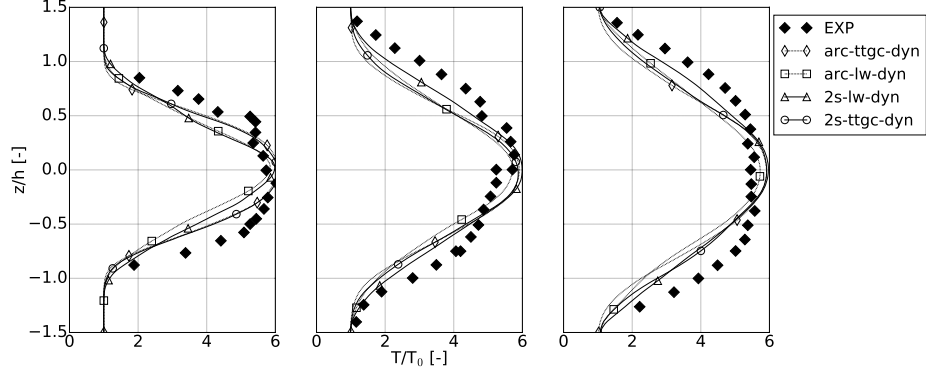


Figure 16: *Transverse profiles of the normalized mean temperature at measurement planes x_4 , x'_4 and x'_5 on Fig. 5.*

Figure 17 compares transverse profiles of the normalized RMS temperature with experimental measurements. RMS maximum values are well captured by all runs but not the minimum values at x_2 and x_5 , indicating that the level of turbulent fluctuation may be too low in the LES near the flame holder (where $y^+ \approx 25$). Note that during experiments, the burner wall elements were water cooled at an unprovided temperature. This may explain discrepancies between measurements and numerical results where adiabatic wall boundary conditions are applied.

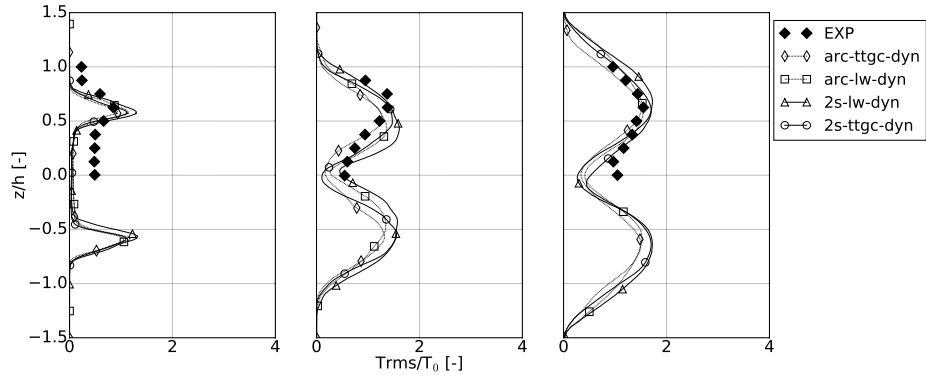


Figure 17: *Transverse profiles of the normalized RMS temperature at measurement planes x_2 , x_4 and x_5 on Fig. 5.*

Figures 18-21 show averaged axial velocity and temperature iso-contours for all runs using the dynamic model. The shaded area corresponds to a zone where the mean heat release is higher than 60 MW/m^3 . Using the LW numerical scheme (Fig. 18 vs Fig. 19 for two-step chemistry or Fig. 20 vs Fig. 21 for ARC), leads to a larger reaction zone closer to the central line $z = 0.06 \text{ m}$, for both chemical schemes. This closer reaction zone to the central line may lead to flame fronts interactions. When using complex chemistry (*arc - ttgc - dyn*, Fig. 21), and compared to the two-step mechanism (*2s - ttgc - dyn*, Fig. 19), the flame brush is thinner and attached to the bluff-body. This observation is coherent with results obtained in Fig. 2: flame response to stretch is overestimated when using the two-step chemical scheme. As a consequence, a two-step flame front will not be able to stabilize itself in regions of high stretch, which is probably the case downstream of the bluff-body.

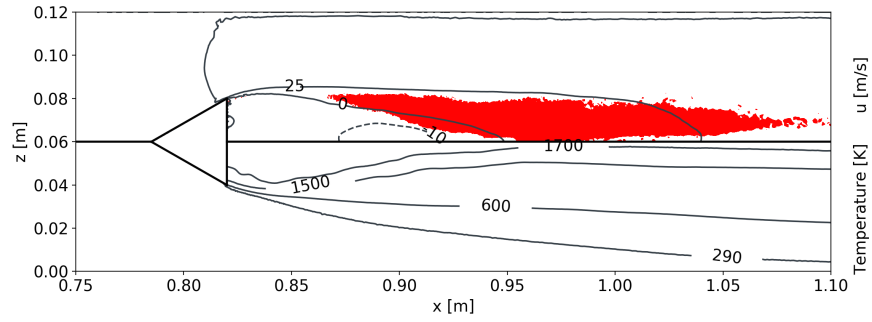


Figure 18: Mean iso-contours of axial velocity (top) and temperature (bottom) of case 2s – lw – dyn, (side view). The red shaded area corresponds to a zone where heat release: $hr \geq 60 \text{ MW/m}^3$.

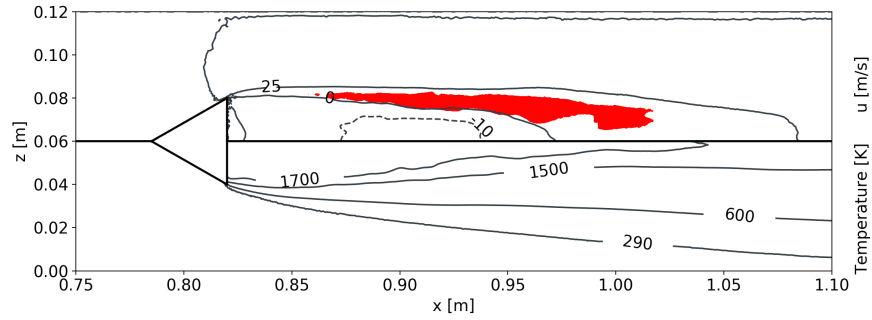


Figure 19: Mean iso-contours of axial velocity (top) and temperature (bottom) of case 2s – ttgc – dyn, (side view). The red shaded area corresponds to a zone where heat release: $hr \geq 60 \text{ MW/m}^3$.

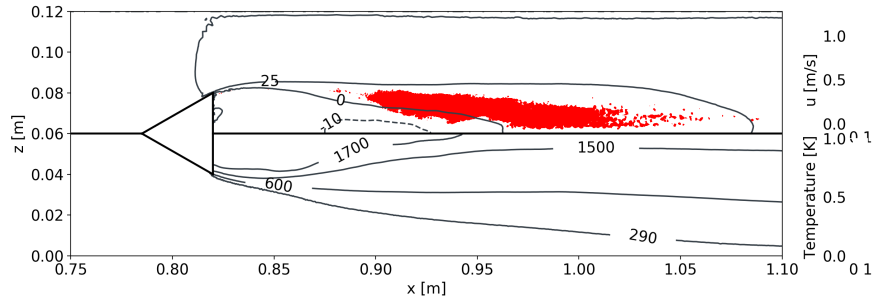


Figure 20: Mean iso-contours of axial velocity (top) and temperature (bottom) of case arc – lw – dyn, (side view). The red shaded area corresponds to a zone where heat release: $hr \geq 60 \text{ MW/m}^3$.

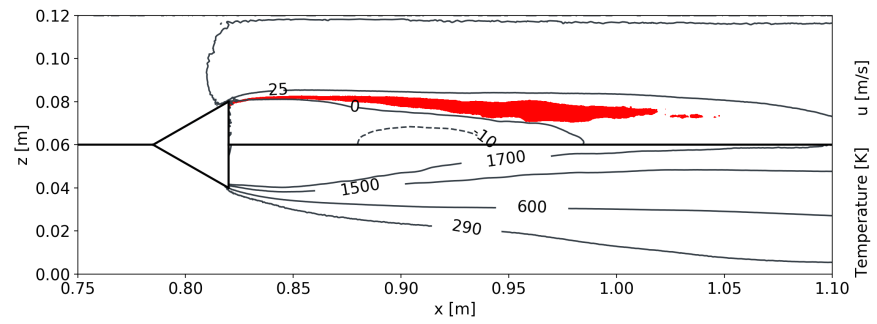


Figure 21: Mean iso-contours of axial velocity (top) and temperature (bottom) of case arc – ttgc – dyn, (side view). The red shaded area corresponds to a zone where heat release: $hr \geq 60 \text{ MW/m}^3$.

Simulations	η
<i>2s - lw - dyn</i>	0.418
<i>2s - ttgc - dyn</i>	0.401
<i>arc - lw - dyn</i>	0.419
<i>arc - ttgc - dyn</i>	0.399

Table 5: Volvo simulated cases efficiencies η

Figures 18-21 suggest that combustion is far from complete for this operating point. This was checked by computing the efficiency η :

$$\eta = 1 - \frac{\int_{outlet} \rho Y_{Fuel} u \cdot dy \cdot dz}{\int_{inlet} \rho Y_{Fuel} u \cdot dy \cdot dz} \quad (13)$$

For all cases, η does not exceed $\eta \approx 0.42$: more than half of the injected fuel has not burnt and exits the burner. This is very different from gas turbine chambers where values of η of the order of 0.99 are expected. Table 5 also shows that efficiencies are higher when using LW numerical scheme, pointing out again that the spatial accuracy of the code affects overall results. No experimental data is available for η .

7. Conclusion

This paper has described the effects of three simulation elements: (1) chemistry description, (2) subgrid scale flame / turbulence interaction and (3) spatial accuracy of the numerical method, on Large Eddy Simulation of the turbulent premixed flame of the VOLVO rig [21–23]. Results show that going from global two-step chemistry to an analytically reduced chemistry (ARC) using 22 independent species improves the simulation accuracy. Similarly, going from a static SGS model for flame-turbulence interaction to a fully dynamic model as proposed by Charlette et al. [46] improves results too but, more importantly, avoids the need for the user to specify the fractal dimension of the model which is determined, automatically and locally, by the dynamic procedure. Finally, the order

of accuracy of the numerical method also plays a significant role, probably because it captures the growth rates of hydrodynamic instabilities along the flame front with more accuracy: results obtained with the 3rd order TTGC scheme [26] are also better than those obtained with the second order Lax-Wendroff scheme. In conclusion, this paper confirms that high-order spatial numerical methods combined with dynamic SGS models and analytically reduced chemistry can be used to simulate turbulent flames and that these ingredients should now be applied to more complex flames.

Acknowledgments

This work was performed using HPC resources from GENCI-CINES (Dari 2016-2b7525). The authors thank the support of Safran Helicopter Engines (Dr. S. Richard) and ANRT/CIFRE.

- [1] P. Pepiot, Automatic strategies to model transportation fuel surrogates, Ph.D. thesis, Stanford University (2008).
- [2] P. Volpiani, T. Schmitt, D. Veynante, A posteriori tests of a dynamic thickened flame model for large eddy simulations of turbulent premixed combustion, *Combust. Flame* 174 (2016) 166–178.
- [3] P. S. Volpiani, T. Schmitt, D. Veynante, Large eddy simulation of a turbulent swirling premixed flame coupling the TFLES model with a dynamic wrinkling formulation, *Combust. Flame* 180 (2017) 124–135.
- [4] F. Charlette, D. Veynante, C. Meneveau, A power-law wrinkling model for LES of premixed turbulent combustion: Part I - non-dynamic formulation and initial tests, *Combust. Flame* 131 (2002) 159–180.
- [5] O. Colin, M. Rudgyard, Development of high-order taylor-galerkin schemes for unsteady calculations, *J. Comput. Phys.* 162 (2) (2000) 338–371.
- [6] P. D. Lax, B. Wendroff, Difference schemes for hyperbolic equations with high order of accuracy, *Commun. Pure Appl. Math.* 17 (1964) 381–398.
- [7] P. A. T. Cocks, M. C. Soteriou, V. Sankaran, Impact of numerics on the predictive capabilities of reacting flow LES, *Combust. Flame* 162 (2015) 3394–3411.
- [8] K. N. C. Bray, The interaction between turbulence and combustion, in: 17th Symp. (Int.) on Combustion, The Combustion Institute, Pittsburgh, 1979, pp. 223–233.
- [9] N. Peters, *Turbulent combustion*, Cambridge University Press, 2001.
- [10] F. A. Williams, *Combustion Theory*, Benjamin Cummings, Menlo Park, CA, 1985.
- [11] T. Poinso, D. Veynante, *Theoretical and Numerical Combustion*, Third Edition (www.cerfacs.fr/elearning), 2011.

- [12] H. Pitsch, Large eddy simulation of turbulent combustion, *Ann. Rev. Fluid Mech.* 38 (2006) 453–482.
- [13] P. Moin, S. V. Apte, Large-eddy simulation of realistic gas turbine combustors, *AIAA Journal* 44 (4) (2006) 698–708.
- [14] N. Gourdain, L. Gicquel, G. Staffelbach, O. Vermorel, F. Duchaine, J.-F. Boussuge, T. Poinsot, High performance parallel computing of flows in complex geometries - part 2: applications, *Comput. Sci. Disc.* 2 (1) (2009) 28pp.
- [15] W. Meier, P. Weigand, X. Duan, R. Giezendanner-Thoben, Detailed characterization of the dynamics of thermoacoustic pulsations in a lean premixed swirl flame, *Combust. Flame* 150 (1-2) (2007) 2–26.
- [16] S. Roux, G. Lartigue, T. Poinsot, U. Meier, C. Bérat, Studies of mean and unsteady flow in a swirled combustor using experiments, acoustic analysis and large eddy simulations, *Combust. Flame* 141 (2005) 40–54.
- [17] B. Franzelli, E. Riber, L. Y. Gicquel, T. Poinsot, Large eddy simulation of combustion instabilities in a lean partially premixed swirled flame, *Combust. Flame* 159 (2) (2012) 621–637.
- [18] V. Moureau, P. Domingo, L. Vervisch, D. Veynante, DNS analysis of a $Re=40000$ swirl burner, in: N. A. U. Center for Turbulence Research (Ed.), *Proc. of the Summer Program*, no. 13, 2010, pp. 209–298.
- [19] V. Moureau, P. Domingo, L. Vervisch, From large-eddy simulation to direct numerical simulation of a lean premixed swirl flame: Filtered laminar flame-pdf modeling, *Combust. Flame* 158 (7) (2011) 1340–1357.
- [20] J.-M. Lourier, M. Stohr, B. Noll, S. Werner, A. Fiolitakis, Scale adaptive simulation of a thermoacoustic instability in a partially premixed lean swirl combustor, *Combust. Flame* 183 (2017) 343–357.

- [21] A. Sjunnesson, C. Nelsson, E. Max, LDA Measurements of velocities and turbulence in a bluff body stabilized flame, 4th International Conference on Laser Anemometry - Advances and Application, ASME 3 (1991) 83–90.
- [22] A. Sjunnesson, P. Henrikson, CARS measurements and visualization of reacting flows in a bluff body stabilized flame, 28th Joint Propulsion Conference and Exhibit, AIAA 92-3650.
- [23] A. Sjunnesson, S. Olovsson, B. Sjöblom, Validation Rig-A tool for flame studies, 10th International Symposium on Air Breathing Engines (1991) 385–393.
- [24] A. Ghani, T. Poinso, L. Gicquel, G. Staffelbach, LES of longitudinal and transverse self-excited combustion instabilities in a bluff-body stabilized turbulent premixed flame, *Combust. Flame* 162 (2015) 4075–4083.
- [25] N. Zettervall, K. Nordin-Bates, E. J. K. Nilsson, C. Fureby, Large Eddy Simulation of a premixed bluff body stabilized flame using global and skeletal reaction mechanisms, *Combust. Flame* (2017) 1–22.
- [26] O. Colin, F. Ducros, D. Veynante, T. Poinso, A thickened flame model for large eddy simulations of turbulent premixed combustion, *Phys. Fluids* 12 (7) (2000) 1843–1863.
- [27] T. Jaravel, E. Riber, B. Cuenot, G. Bulat, Large eddy simulation of an industrial gas turbine combustor using reduced chemistry with accurate pollutant prediction, *Proc. Combust. Inst.* 36 (2016) 3817–3825.
- [28] A. Felden, Development of analytically reduced chemistries and applications in large eddy simulations of turbulent combustion, Ph.D. thesis, Ecole Doctorale MEGeP - INPT TOULOUSE (2017).
- [29] K. K. Kuo, Principles of combustion, 2nd Edition, John Wiley & Sons, Inc., 2005.

- [30] S. Jerzembeck, N. Peters, P. Pepiot-desjardins, H. Pitsch, Laminar burning velocities at high pressure for primary reference fuels and gasoline : Experimental and numerical investigation, *Combust. Flame* 156 (2) (2009) 292–301.
- [31] H. Curran, P. Gaffuri, W. Pitz, C. Westbrook, A Comprehensive Modeling Study of n-Heptane Oxidation, *Combust. Flame* 114 (1) (1998) 149–177.
- [32] H. Curran, P. Gaffuri, W. Pitz, C. Westbrook, A comprehensive modeling study of iso-octane oxidation, *Combust. Flame* 129 (3) (2002) 253–280.
- [33] P. Pepiot-Desjardins, H. Pitsch, An efficient error-propagation-based reduction method for large chemical kinetic mechanisms, *Combust. Flame* 154 (2008) 67–81.
- [34] T. Lvs, D. Nilsson, F. Mauss, Automatic reduction procedure for chemical mechanisms applied to premixed methane/air flames, in: 28th Symp. (Int.) on Comb., no. 2, 2000, pp. 1809–1815.
- [35] K. Bray, M. Champion, P. Libby, Mean reaction rates in premixed turbulent flames, in: 22nd Symp. (Int.) on Comb., 1988, pp. 763–769.
- [36] K. N. C. Bray, Studies of the turbulent burning velocity, *Proc. R. Soc. Lond. A* 431 (1990) 315–335.
- [37] N. Swaminathan, K. Bray, *Turbulent Premixed Flames*, Cambridge University Press, 2011.
- [38] J. A. van Oijen, F. A. Lammers, L. P. H. de Goey, Modeling of premixed laminar flames using flamelet generated manifolds, *Combust. Sci. Tech.* 127 (2001) 2124–2134.
- [39] B. Fiorina, O. Gicquel, L. Vervisch, S. Carpentier, N. Darabiha, Approximating the chemical structure of partially-premixed and diffusion counter-flow flames using FPI flamelet tabulation, *Combust. Flame* 140 (2005) 147–160.

- [40] M. A. Singer, S. B. Pope, Exploiting ISAT to solve the equations of reacting flow, *Combust. Theory and Modelling* 8 (2) (2004) 361–383.
- [41] D. Veynante, V. Moureau, Analysis of dynamic models for large eddy simulations of turbulent premixed combustion, *Combust. Flame* 162 (12) (2015) 4622–4642.
- [42] G. Wang, M. Boileau, D. Veynante, Implementation of a dynamic thickened flame model for large eddy simulations of turbulent premixed combustion, *Combust. Flame* 158 (11) (2011) 2199–2213.
- [43] G. Wang, M. Boileau, D. Veynante, K. Truffin, Large eddy simulation of a growing turbulent premixed flame kernel using a dynamic flame surface density model, *Combust. Flame* 159 (8) (2012) 2742–2754.
- [44] P. Quillatre, Simulation aux grandes échelles d’explosions en domaine semi-confiné, Ph.D. thesis, Ecole Doctorale MEGeP - INPT TOULOUSE (2014).
- [45] T. D. Butler, P. J. O’Rourke, A numerical method for two-dimensional unsteady reacting flows, in: 16th Symp. (Int.) in Comb., no. 1, The Combustion Institute, 1977, pp. 1503–1515.
- [46] F. Charlette, C. Meneveau, D. Veynante, A Power-Law Flame Wrinkling Model for LES of Premixed Turbulent Combustion Part II: Dynamic Formulation, *Combust. Flame* 197 (2002) 181–197.
- [47] G. Kuenne, A. Ketelheun, J. Janicka, LES modeling of premixed combustion using a thickened flame approach coupled with FGM tabulated chemistry, *Combust. Flame* 158 (9) (2011) 1750 – 1767.
- [48] J.-P. L egier, Simulations num eriques des instabilit es de combustion dans les foyers a eronautiques, Phd thesis, Ecole Doctorale MEGeP - INPT TOULOUSE (2001).
- [49] F. Nicoud, H. Baya Toda, O. Cabrit, S. Bose, J. Lee, Using singular values to build a subgrid-scale model for large eddy simulations, *Phys. Fluids* 23 (8) (2011) 085106.

- [50] T. Schmitt, M. Boileau, D. Veynante, Flame Wrinkling Factor Dynamic Modeling for Large Eddy Simulations of Turbulent Premixed Combustion, *Flow, Turb. and Combustion* (2015) 199–217.
- [51] F. Gouldin, K. Bray, J. Y. Chen, Chemical closure model for fractal flamelets, *Combust. Flame* 77 (1989) 241–259.
- [52] O. Gulder, Turbulent premixed flame propagation models for different combustion regimes, in: 23rd Symp. (Int.) on Comb., no. 1, The Combustion Institute, Pittsburgh, Orleans, 1991, pp. 743–750.
- [53] P. Quillatre, O. Vermorel, T. Poinsot, P. Ricoux, Large eddy simulation of vented deflagration, *Industrial & Engineering Chemistry Research* 52 (33) (2013) 11414–11423.
- [54] S. Mouriaux, O. Colin, D. Veynante, Adaptation of a dynamic wrinkling model to an engine configuration, *Proc. Combust. Inst.* 36 (3) (2017) 3415–3422.
- [55] M. Germano, A proposal for a redefinition of the turbulent stresses in the filtered Navier-Stokes equations, *Phys. Fluids* 29 (7) (1986) 2323–2324.
- [56] M. Germano, U. Piomelli, P. Moin, W. Cabot, A dynamic subgrid-scale eddy viscosity model, *Phys. Fluids* 3 (7) (1991) 1760–1765.
- [57] M. Germano, Turbulence: the filtering approach, *J. Fluid Mech.* 238 (1992) 325–336.
- [58] D. K. Lilly, A proposed modification of the germano sub-grid closure method, *Phys. Fluids* 4 (3) (1992) 633–635.
- [59] D. Veynante, T. Schmitt, M. Boileau, Analysis of dynamic models for turbulent premixed combustion, *Proc. of the Summer Program* (2012) 387–396.
- [60] F. Rayleigh, On the resultant of a large number of vibrations of the same pitch and of arbitrary phase, *Philosophical Magazine* 10 (60) (1880) 73–78.

- [61] T. Schönfeld, M. Rudgyard, Steady and unsteady flows simulations using the hybrid flow solver AVBP, *AIAA Journal* 37 (11) (1999) 1378–1385.
- [62] H. Li, P. Khare, H. Sung, V. Yang, A Large-Eddy-Simulation Study of Combustion Dynamics of Bluff-Body Stabilized Flames, *Combust. Sci. Tech.* 188 (6) (2016) 924–952.
- [63] J. Kim, S. B. Pope, Effects of combined dimension reduction and tabulation on the simulations of a turbulent premixed flame using a large-eddy simulation/probability density function method, *Combust. Theory and Modelling* 18.
- [64] H. Wu, P. C. Ma, Y. Lv, M. Ihme, MVP-Workshop Contribution: Modeling of Volvo Bluff Flame Experiment, *AIAA Journal* 55 (2017) 1–16.
- [65] T. Poinso, S. Lele, Boundary conditions for direct simulations of compressible viscous flows, *J. Comput. Phys.* 101 (1) (1992) 104–129.
- [66] N. Guezennec, T. Poinso, Acoustically nonreflecting and reflecting boundary conditions for vorticity injection in compressible solvers, *AIAA Journal* 47 (2009) 1709–1722.